JMEPEG (2010) 19:1256–1263
DOI: 10.1007/s11665-010-9625-1

1059-9495/$19.00

An Investigation into Microstructures and Mechanical Properties of AA7075-T6 during Friction Stir Welding at Relatively High Rotational Speeds

T. Azimzadegan and S. Serajzadeh

(Submitted October 9, 2009; in revised form January 17, 2010)

In this study, microstructural changes and mechanical properties during friction stir welding of AA7075-T6 have been investigated. Friction stir welding at relatively high rotational speeds ranging from 1000 to 1400 rpm and longitudinal speeds in the range of 40 to 80 mm/min have been performed and then microstructures and mechanical properties of the weldments have been studied. The results show that the rotational and longitudinal speeds have a significant effect on the microstructures as well as the mechanical behavior of the welded material while a fine grain structure is produced at higher ratio of rotational speed to longitudinal speed. On the other hand, for a given longitudinal speed, it is revealed that there is an optimum rotational speed which gives the highest tensile strength and elongation for the stirred zone.

Keywords 7075 aluminum alloy, friction stir welding, mechanical properties, microstructures

1. Introduction

Friction stir welding (FSW) is a relatively new route to conduct welding operations in solid-sate conditions (Ref 1). During the process, a rotating pin is first inserted in the material and after a dwell time, it moves along the joint line. Friction between the rotating tool and the workpiece generates heat which reduces the flow stress of material around the rotating pin and tool shoulder, and then weld joint is produced by material flow from the advancing side to the retreating side of the weldment.

Several researches have been conducted to characterize the relationship between microstructures and mechanical properties in aluminum alloys. For instance, Rhodes et al. (Ref 2) and Mahoney et al. (Ref 3) have shown that the significant changes occur in microstructures and dislocation structures of the weld nugget in FSW of AA7075, leading to an decrease in the ultimate tensile strength. Hassan et al. (Ref 4) have studied the effect of the welding conditions on the final microstructures and the mechanical properties of the stir zone in welding of AA7010 plates. They have shown that at low heat inputs, higher hardness and larger grain size were produced at the top of the nugget. Investigation into the mechanical properties of the friction stir-welded joints in AA2017-T351 has been conducted by Liu et al. (Ref 5). They have reported that significant material softening may be occurred due to the coarsening of fine precipitates within the welded and heat-affected regions. In a similar work, Barcellona et al. (Ref 6) have reported that the average value of the ultimate tensile strength is reduced to about 75% of the ultimate tensile strength of the base material in AA 7075-T6 owing to material softening from coarsening of fine precipitates. Cavaliere et al. (Ref 7, 8) have studied FSW of AA 2024 and AA7075 and reported formation of the onion ring structure in the weld nugget. Su et al. (Ref 9) have found that the grain structure are strongly dependent on the tool design, processing parameters, and cooling rate in the FSW of AA7075-T6. Jata et al. (Ref 10) have investigated the effect of FSW on the microstructures and mechanical properties of AA7050-T7451 joints and reported that the size of the strengthening precipitates and the precipitate-free zone is increased by a factor of 5. Sato et al. (Ref 11) have investigated microstructural distribution in FSW of AA6063 using hardness testing associating with different microscopy techniques. In addition, thermal and mechanical modeling of FSW of aluminum alloys have been performed in several researches utilizing different numerical techniques such as the finite element method (Ref 12-14).

Previous researches on microstructure evolution and mechanical properties during FSW of AA7xxx have been mainly performed under relatively low rotational speeds, i.e., 180 to 350 rpm, and therefore the effect of higher rotational speeds on the microstructures and mechanical properties of FSW-7075 joints has not been clearly reported yet. On the other hand, higher rotational speed makes it possible for higher production rate. Thus, this study has been concentrated on the mechanical properties and the microstructures development during and after FSW AA7075-T6 at high rotational speeds in the range of 1000 to 1400 rpm.

Different testing techniques such as optical and scanning electron microscopy, hardness, and tensile testing are then used to evaluate the microstructures and mechanical properties of welded material.

T. Azimzadegan and **S. Serajzadeh**, Department of Materials Science and Engineering, Sharif University of Technology, Azadi Ave., Tehran, Iran. Contact e-mail: serajzadeh@sharif.edu.

2. Experimental

The composition the employed aluminum alloy is given in Table 1. FSW was performed on a 5 mm thick plate with 100 mm in length, along the welding line, and 50 mm in width. The welding tool is made of H13 tool steel with a hardness of 52 HRC having shoulder height of 10 mm and diameter of 20 mm. The shoulder face was designed as a concave cone, while the inside angle of the rotating tool was about 82°. The welding tool was tilted 3° about vertical axis, and a cylindrical welding pin was employed in the experiments. The diameter of the pin was 6 mm, and the pin height was 4.9 mm. The range of rotational speeds utilized for the welding was varied between 1000 and 1400 rpm, whereas the longitudinal speeds were varied from 40 to 80 mm/min (0.67 to 1.3 mm/s). Temperature measurements were also made on the welded joint during the process by means of thermocouples placed at distances of 5 and 25 mm from the centerline of weld. Thermocouples were attached to a data acquisition system at the rate of 10 Hz, and data collection was accomplished with the system attached to a personal computer. The microstructural studies were made utilizing optical and scanning electron microscopy. After welding, the samples were sectioned normal to the welding direction and then prepared by grinding disks and polished and finally etched with Keller's reagent: 150 mL H_2O, 3 mL HNO_3, 6 mL HCl, and 6 mL HF (Ref 15).

To evaluate the mechanical properties of the welded part, longitudinal and transverse tensile tests were also performed. Tensile tests for the material within the nugget zone as well as the hardness testing were carried out 3 weeks after the welding experiments. However, tensile tests for heat-affected zone (HAZ) were performed 6 months after welding operation to ensure a stable state of natural aging in the above region. Longitudinal tensile specimens with a gage length of 32 mm and width of 6 mm were machined out of the nugget zone while the axis of the samples coinciding with the center of the nugget. Transverse tensile specimens were 100 mm long with a rectangular cross section, 5 by 6 mm, and a 32 mm gage section. Tensile tests were performed at room temperature at the strain rate of 10^{-3} s^{-1} using an Instron machine. Vickers hardness measurements were conducted at mid-thickness across the welds with the distance of about 2 mm between the selected points, while in the hardness tests, 30 N load and holding time of 30 s were employed.

3. Results and Discussion

The effects of the rotational speeds on the weld pool geometry as well as the weld quality are displayed in Fig. 1, for a longitudinal speed of 40 mm/min. As the rotational speed is increased from 1000 to 1400 rpm, the stir zone was widely extended. The weld joint constructed with a rotational speed of 1300 rpm makes defect-free weld as observed in Fig. 1(c), while for the other welding speeds, it is possible to observe void-like or wormhole defects in the weld zone as shown in Fig. 1. It should be noted that the creation of some defects during FSW may be attributed to discontinuities in the velocity field around the rotating tool. As the material flows around the advancing side of the pin, it may correspond to high or low rotational speeds, resulting in a typical defect known as a tunnel or wormhole. In fact, when material passes around the advancing side of the weld, there is no force promoting its movement back into the volume stirred by the moving tool.

It is observed that the flow lines within the weld nugget are formed as the material layers undergo different levels of plastic deformation at different positions of the weld (Ref 16). The flow pattern on the transverse cross-section is often in the form of onion rings. The spacing between the layers equals the distance traveled by the welding tool in one revolution. In this study, it was found that the higher the rotational speed, the smaller is the distance between the onion rings. Also, this pattern near the top surface has not been observed.

The appearance of voids developed during welding is shown in Fig. 2. It can be found that the joint under longitudinal

Table 1 The chemical composition of the employed alloy

Elements	Al	Zn	Mg	Cu	Cr
Wt.%	90.07	5.6	2.5	1.6	0.23

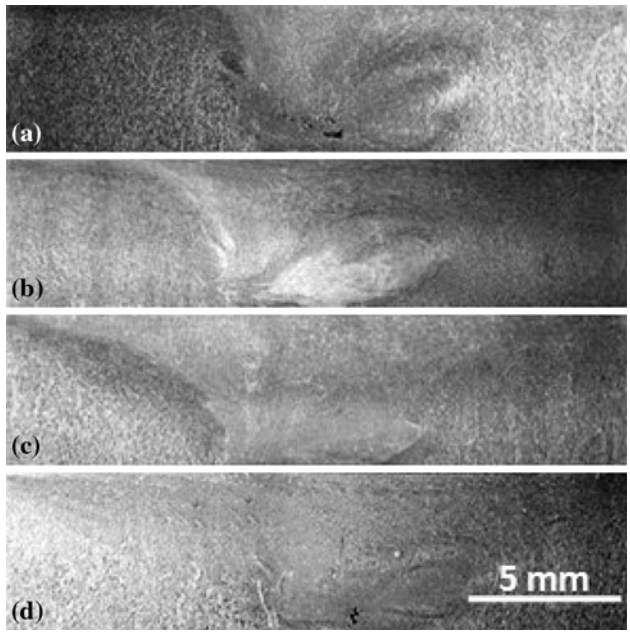

Fig. 1 Effect of rotational speed on weld pool geometry at longitudinal speed of 40 mm/min: (a) 1000, (b) 1200, (c) 1300, and (d) 1400 rpm

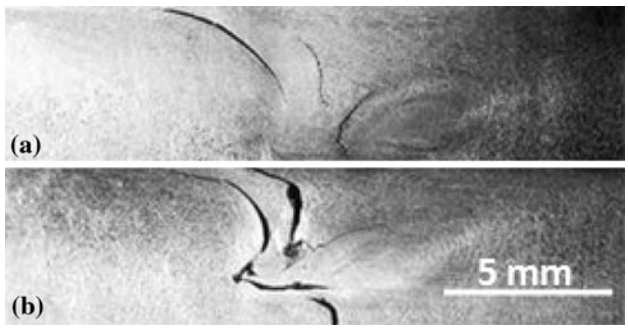

Fig. 2 Defect appearance within the welded samples: (a) rotational speed of 1300 rpm and longitudinal speed of 60 mm/min and (b) rotational speed of 1000 rpm and longitudinal speed of 80 mm/min

speeds of 60 and 80 mm/min and rotational speeds of 1300 and 1000 rpm, respectively, has not produced a sound weld. Note that in Fig. 2(b), a relatively large section of material of about 1 mm thickness at the bottom side was not affected during welding. It can be seen that increasing the longitudinal speed as the heat input is decreased causes reduction in the width of the weld. Therefore, it shows that the amount of heat input plays an important role on the shape of deformation zone.

Figure 3 illustrates optical microstructures of the base material containing strengthening precipitates. Grain structures in the nugget zone were investigated to reveal the effect of welding speed on microstructural evolution using optical metallography and SEM. Figure 4 and 5 shows the variations

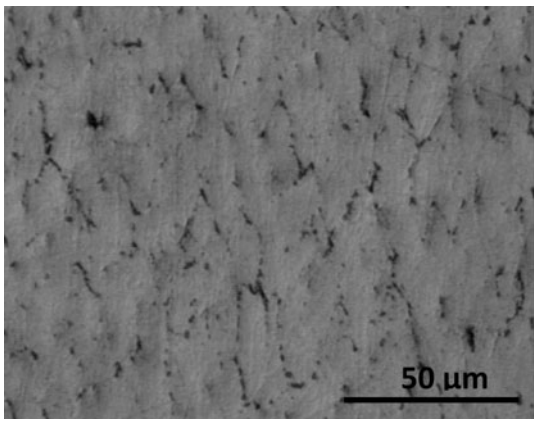

Fig. 3 Optical micrograph of the base material

of grain size and its distribution in the welded 7075-T6 under the rotation speeds of 1200 and 1300 rpm. Both welds exhibit an equiaxed grain structure in the weld nugget. In the high rotational speeds, grains near the crown and root regions are smaller than the grains in the central region of the weld nugget. Grain refinement induced by FSW is related to the stirring effect of the rotating pin that leads to dynamic recrystallization owing to the concurrent effects of frictional heating and plastic deformation. The size of dynamically recrystallized grain may be determined as follows (Ref 17):

$$d^{-1} = a + b\ln(Z), \quad \text{(Eq 1)}$$

where d is the grain diameter, a and b are constitutive constants, and Z is the Zener-Hollomon parameter which is expressed as

$$Z = \dot{\varepsilon}\exp\left(\frac{Q}{RT}\right), \quad \text{(Eq 2)}$$

where Q is the activation energy and R is the gas constant. With regard to Eq 1 and 2, smaller grain size is produced during dynamic recrystallization when imposed Z-parameter is higher. Accordingly, in the root weld, grain size is smaller due to lower temperature in this area because of the effect of backing plate as heat sink and, on the other hand, small grains are produced in the bottom of shoulder where large strain rates are imposed to the deforming material which leads to high Z-parameter.

As seen in Fig. 6, a fine equiaxed grain structure on the order of 2 to 14 µm in diameter is present in the nugget zone. The very small grain structures formed in the nugget zone may be the result of continuous dynamic recrystallization under

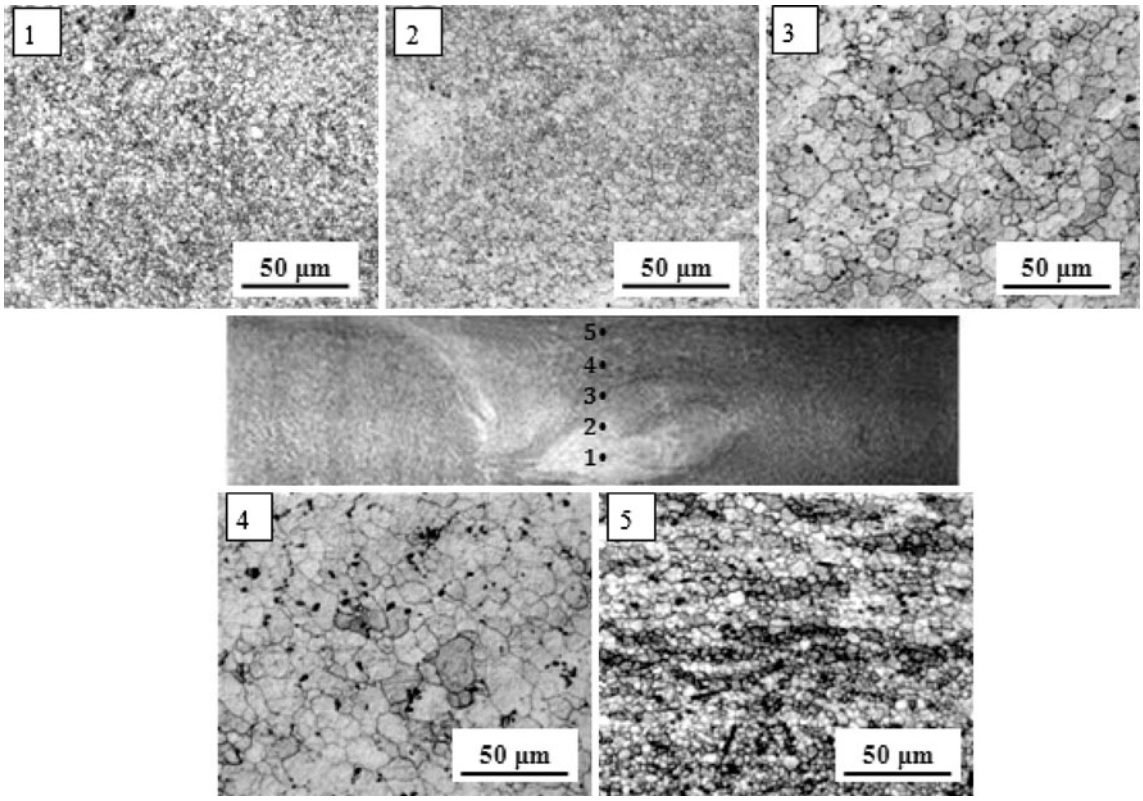

Fig. 4 Grain size distribution along thickness direction in 7075-T6 Al alloy for rotational speed of 1200 rpm and longitudinal speed of 40 mm/min

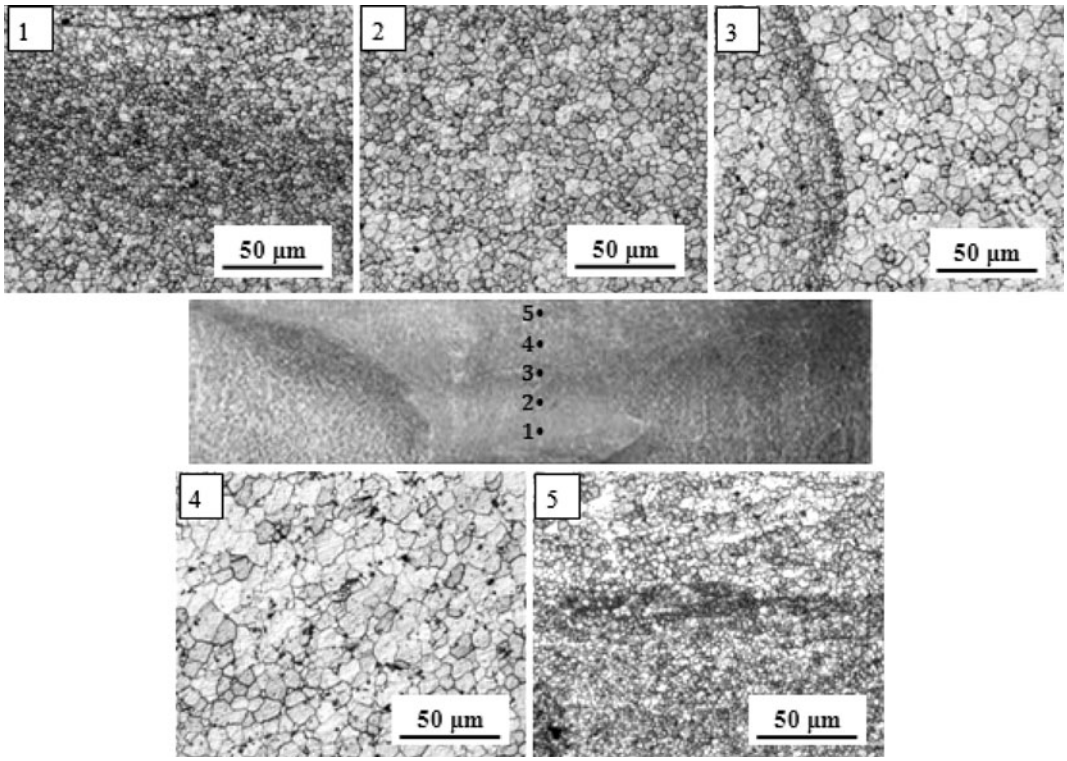

Fig. 5 Grain size distribution along thickness direction in 7075-T6 Al alloy for rotational speed of 1300 rpm and longitudinal speed of 40 mm/min

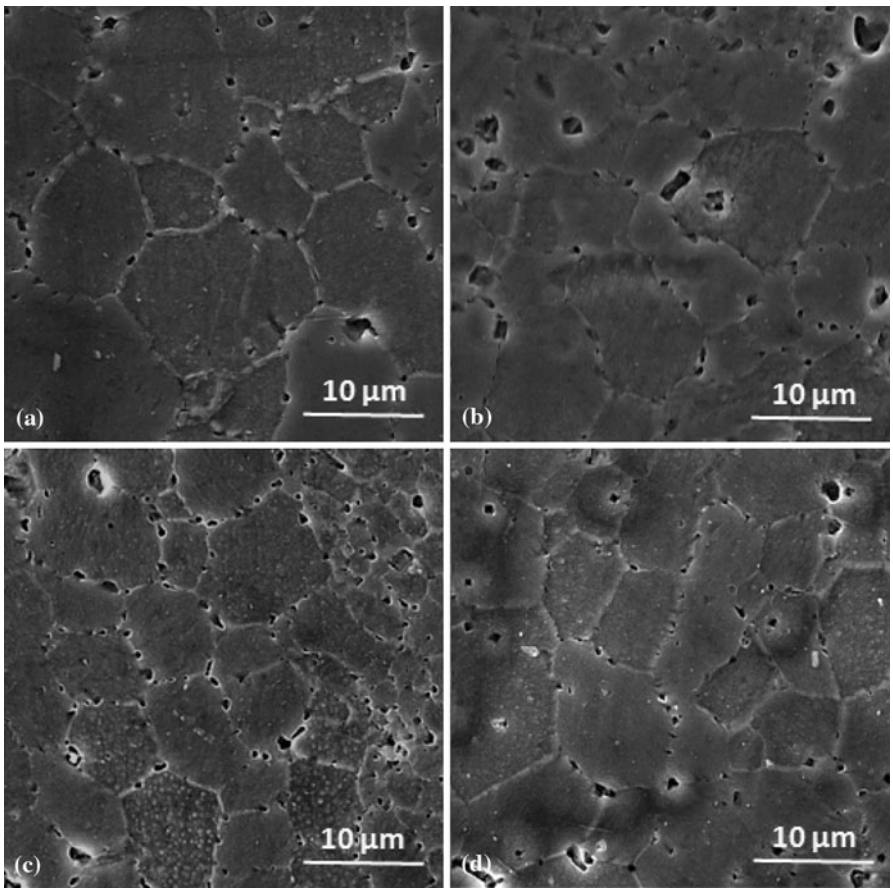

Fig. 6 SEM micrographs of the nugget zone at different rotational and longitudinal speeds: (a) 1000 rpm and 40 mm/min, (b) 1000 rpm and 80 mm/min, (c) 1300 rpm and 40 mm/min, and (d) 1300 rpm and 60 mm/min

extremely large deformation, high strain rates, and high temperature (Ref 9). Maximum temperatures measured by thermocouple are listed in Table 2. Unlike the FSW at lower rotational speeds (Ref 4), for a given longitudinal speed, the grain size is reduced with increasing the rotational speed from 1000 to 1300 rpm, although heat input is increased. This implies that the recrystallized grain size of the employed alloys is more sensitive to strain rate than recrystallization temperature. It should be noted that at high rotational speeds, as illustrated in Table 2, although the maximum temperature is almost the same, however, strain rate increases with increasing rotational speed. Hence, based on Eq 1, it is expected that grain size in the weld zone is reduced when higher rotational speeds are employed in the welding operation.

Furthermore, at the lower longitudinal speed, i.e., 40 mm/min, microstructures are more homogenous compared to welding speed of 80 mm/min and grain sizes in the nugget zone are very fine being in the range of 2 to 8 μm. However, the grain size increases to 6 to 14 μm when welding speed of 60 mm/min is employed. Therefore, it may be concluded that fine grains are produced at the high ratio of rotational to longitudinal speeds.

The effect of higher and lower ratios of the rotational to longitudinal speed, i.e., high and low heat input, on HAZ microstructures is shown in Fig. 7. For lower heat input, the grain boundary precipitates in the HAZ is roughly coarsened, and therefore it is expected that lower density of fine strengthening precipitates is presented compared to the microstructures produced under higher heat input.

Table 2 Maximum temperatures measured by thermocouple at different welding parameters

Samples no.	Rotational speed, rpm	Longitudinal speed, mm/min	Maximum temperature, °C
1	1000	40	467
2	1000	80	442
3	1200	40	474
4	1300	40	476
5	1300	60	470

Tensile tests have been carried out to evaluate the effect of rotational and longitudinal speeds on the mechanical properties of the nugget zone and HAZ. The stress-strain curves of base material and the weld zone are compared in Fig. 8. In addition, the results of the tensile tests for friction stir-welded 7075-T6 Al alloy are shown in Table 3. The results show a reduction in yield and ultimate tensile strengths in the weld nugget irrespective of the welding speeds. This may be attributed to the elimination of the strengthening precipitates in the weld nugget and the thermomechanically affected zones (Ref 2, 15).

It can be seen that lower and higher rotational speeds greater than 1300 rpm produce the weld metal with lower strength and ductility in comparison with rotational speed of 1300 rpm at a constant longitudinal speed of 40 mm/min. It may be attributed to the formation void-like defects at rotational speeds lower and/or higher than 1300 rpm as discussed earlier. It should be noted that at the optimum rotational speed, the ductility of the weld nugget was greater than that of base material. Also, at the

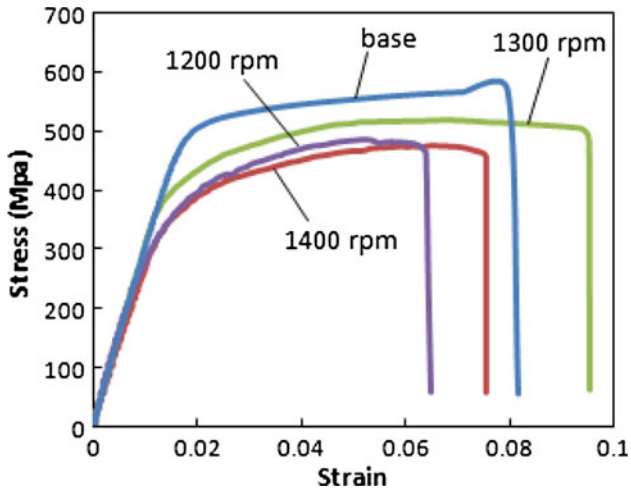

Fig. 8 The stress-strain curves for base and friction stir-welded 7075-T6 Al alloy under different rotational speeds and at constant longitudinal speed of 40 mm/min

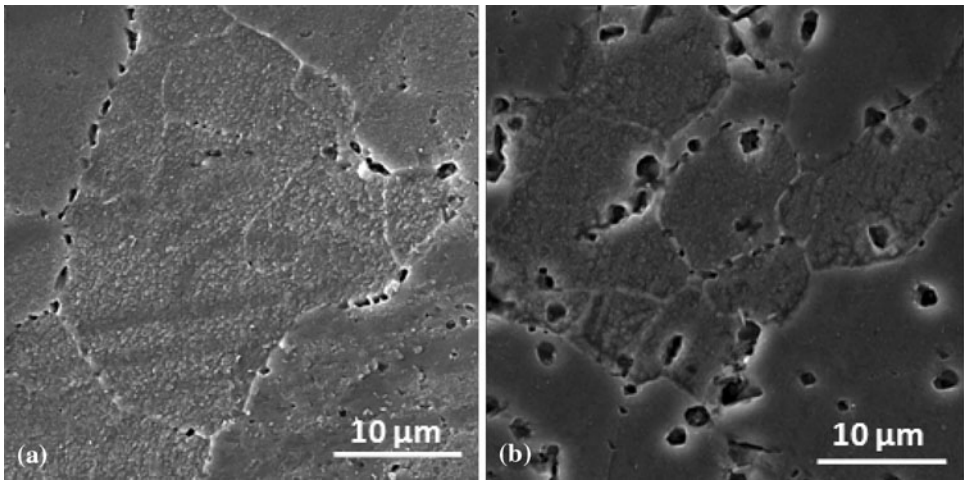

Fig. 7 SEM micrographs of the HAZ at different rotational and longitudinal speeds: (a) 1300 rpm and 40 mm/min and (b) 1000 rpm and 80 mm/min

Table 3 Tensile properties of friction stir-welded 7075-T6 Al alloy

	Longitudinal speed, mm/min	Rotational speed, rpm	Yield strength, MPa	Ultimate tensile strength, MPa	Elongation, %
Base metal	...	...	480	567	8.2
Longitudinal direction of friction stir-welded alloy	40	1200	290	484	6.5
	40	1300	356	518	9.5
	40	1400	290	476	7.5
	60	1300	283	405	7
Transverse direction of friction stir-welded alloy	40	1200	223	385	3
	40	1300	271	430	5.3
	40	1400	215	376	2.8

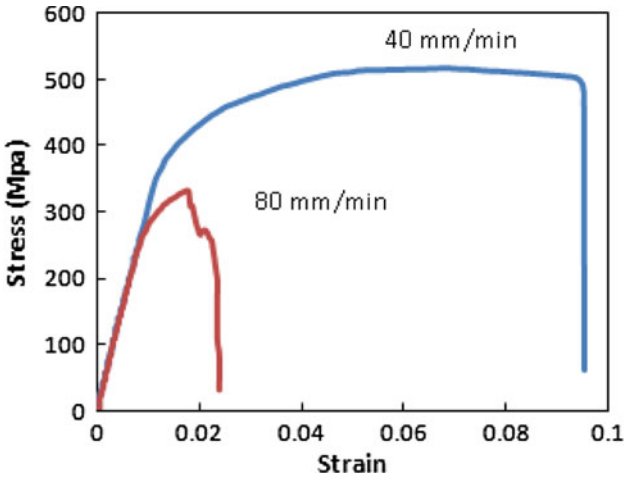

Fig. 9 The stress-strain curves for friction stir-welded 7075-T6 Al alloy with different longitudinal speeds and at constant rotational speed of 1300 rpm

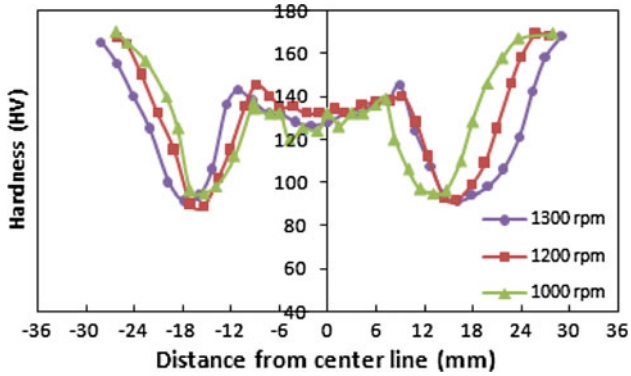

Fig. 10 The hardness profiles measured at mid-thickness region of the welds under different rotational speeds and at constant longitudinal speed of 40 mm/min

rotational speed of 1300 rpm, a longitudinal speed of 40 mm/min leads to much higher yield and tensile strength than a longitudinal speed of 80 mm/min in the nugget zone as shown in Fig. 9.

Overall, from the above observations, it may be found that the differences in mechanical properties of the weld nugget is due to formation of void-like defects as well as the difference in thermal cycles during and after welding which in turn causes re-precipitation and coarsening of strengthening precipitates. In other words, natural aging may occur after the welding process within the weld zone where the severe deformation and thermal cycles have been imposed.

At low heat input, i.e., T_{max} = 442 °C, longitudinal speed of 80 mm/min and rotational speed of 1000 rpm, the tensile strength and ductility are both low owing to the high density of coarse precipitates present on the grain boundaries as shown in Fig. 6(b) and/or formation of voids during welding as shown in Fig. 1. As the heat input increases, i.e., T_{max} = 476 °C, longitudinal speed of 40 mm/min and rotational speed of 1300 rpm, the volume fraction of the coarse precipitates are reduced because of higher temperature of weld zone and dissolving initial precipitates. Therefore, under these circumstances, a relatively large amount of solute is formed in the solution and is available for the subsequent natural aging phenomenon. This leads to an increase in tensile strength as displayed in Fig. 9. On the other hand, as discussed earlier, the weld produced under the above working conditions is defect free and thus the ductility also increases compared to that produced by rotational speed of 1000 rpm.

The hardness profiles under different rotational speeds at constant longitudinal speed of 40 mm/min are shown in Fig. 10. It can be seen that local softening of the material occurs in the weld because of the dissolution of precipitates and the welding thermal cycle do not promote nucleation and growth of all the precipitates. The width of the central plateau in hardness profiles increase with increasing the rotational speeds. Also, the lower hardness values seen in the nugget zone correspond to the rotational speed of 1000 rpm and the hardness values in nugget zone are slightly higher for rotational speed of 1200 rpm than rotational speed of 1300 rpm.

The hardness profiles for different longitudinal speeds at constant rotational speed are plotted in Fig. 11. This figure illustrates that hardness of the weld metal, except for the central region of the weld, is slightly higher for the high longitudinal speed of 80 mm/min. Process parameters such as rotational or longitudinal speed produce different thermal profiles as shown in Fig. 12. The effect of such variations on the precipitation distribution can be investigated. In the weld nugget, for the longitudinal speed of 80 mm/min with a peak temperature equal to 442 °C, according to Fig. 12(a), small $\eta'(MgZn_2)$

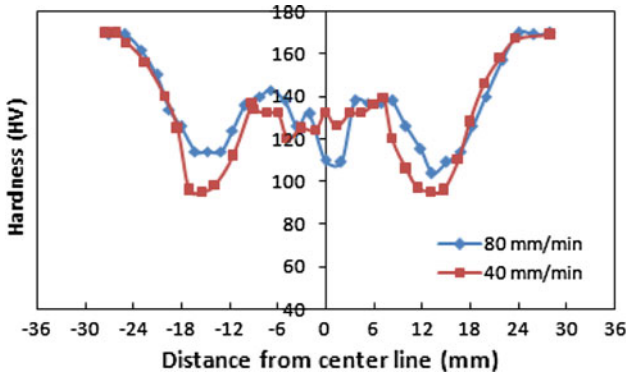

Fig. 11 The hardness profiles measured at mid-thickness region of the welds under different longitudinal speeds and at constant rotational speed of 1000 rpm

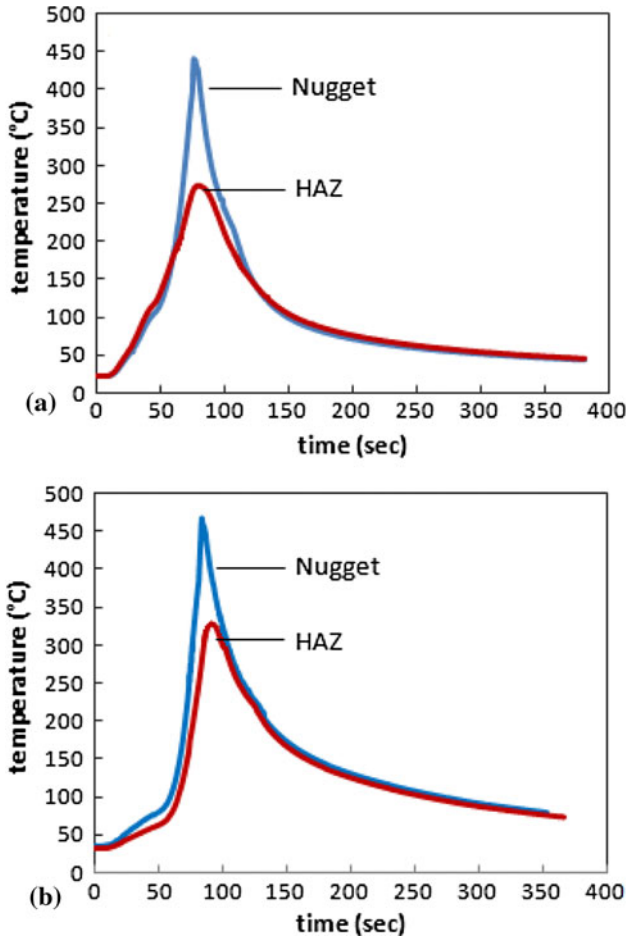

Fig. 12 Measured thermal cycles under different welding speeds: (a) 1000 rpm and 80 mm/min and (b) 1000 rpm and 40 mm/min

precipitates start to dissolve during the heating stage, while coarse η′ transform to η. Regarding the model developed by Kamp et al. (Ref 12), large number of η precipitates dissolves as peak temperature increases, and therefore a low volume fraction of η precipitates and relatively large amount of solute

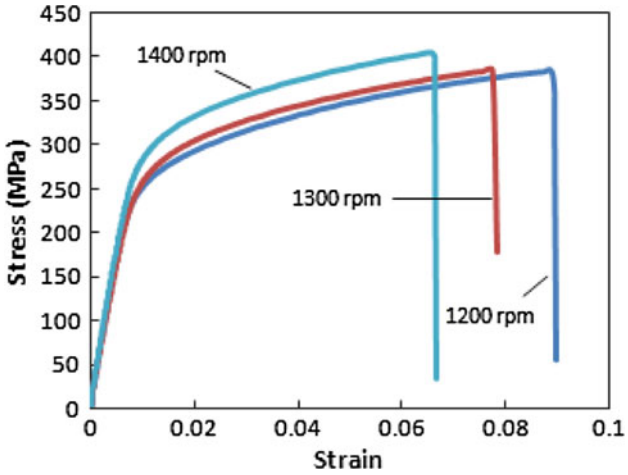

Fig. 13 The stress-strain curves of the HAZ in parallel to weld line under different welding conditions

is left in solution for further precipitation. Whereas welding under longitudinal speed of 40 mm/min produces peak temperature of about 330 °C in HAZ, according to Fig. 12(b), the η′ precipitates may dissolve partially during the heating stage. Therefore, upon cooling, a fine GP zone precipitates may form from the supersaturated solid solution. A greater density of GP zone precipitates are formed as peak temperature increases. In HAZ, for the longitudinal speed of 80 mm/min with peak temperature of about 275 °C, the initial η′ precipitates grow slightly with a very low amount of η being dissolved and therefore the solute remaining in solution is relatively low.

Figure 13 indicates the stress-strain curves of the HAZ in parallel to weld line for different welding parameters. In HAZ, the precipitations are in stable aged conditions as a result of imposed thermal cycle during welding operation. It is observed that for higher heat input, i.e., rotational speed of 1400 rpm, initial precipitates may be partially dissolved, and therefore the material may be naturally aged after welding operation, although the original strength level is never fully regained. As seen in Fig. 13, the yield strength increases by increasing rotational speed.

4. Conclusions

In this article, the effect of high rotational speed on the microstructural changes and the mechanical characteristics of friction stir-welded joints have been investigated. According to the experiments, formation of voids and cracks are quite possible during FSW at high rotational speed. The results show that the weld joint constructed with the rotational speed of 1300 rpm and the longitudinal speed of 40 mm/min can be employed to produce a defect-free weld, revealing that there is an optimum working conditions for producing a sound weld. In addition, for a given longitudinal speed, the grain size in the nugget zone is reduced with increasing the rotational speed. Finally, it has been revealed that there is an optimum rotational speed which gives the highest tensile strength and elongation in which the thermal cycles and aging kinetics are well balanced to provide the appropriate mechanical properties.

References

1. W.M. Thomas, E.D. Nicholas, J.C. Needham, M.G. Murch, P. Templesmith, and C.J. Dawes, Friction Stir Butt Welding, Great Britain Patent 9125978.8, 1991
2. C.G. Rhodes, M.W. Mahoney, W.H. Bingel, R.A. Spurling, and C.C. Bampton, Effects of Friction Stir Welding on Microstructure of 7075 Aluminium, *Scripta Mater.*, 1997, **36**, p 69–75
3. M.W. Mahoney, C.G. Rhodes, J.G. Flintoff, R.A. Spurling, and W.H. Bingel, Properties of Friction-Stir-Welded 7075 T651 Aluminum, *Metall. Mater. Trans. A*, 1998, **29**, p 1955–1964
4. K.A.A. Hassan, P.B. Prangnell, A.F. Norman, D.A. Price, and S.W. Williams, Effect of Welding Parameters on Nugget Zone Microstructure and Properties in High Strength Aluminium Alloy Friction Stir Welds, *Sci. Technol. Weld. Join.*, 2003, **8**, p 257–268
5. H.J. Liu, H. Fujii, M. Maeda, and K. Nogi, Tensile Properties and Fracture Locations of Friction-Stir-Welded Joints of 2017-T351 Aluminum Alloy, *J. Mater. Process. Technol.*, 2003, **142**, p 692–696
6. A. Barcellona, G. Buffa, L. Fratini, and D. Palmeri, On Microstructural Phenomena Occurring in Friction Stir Welding of Aluminium Alloys, *J. Mater. Process. Technol.*, 2006, **177**, p 340–343
7. P. Cavaliere, E. Cerri, and A. Squillace, Mechanical Response of 2024-7075 Aluminium Alloys Joined by Friction Stir Welding, *J. Mater. Sci.*, 2005, **40**, p 3669–3676
8. P. Cavaliere, R. Nobile, F.W. Panella, and A. Squillace, Mechanical and Microstructural Behaviour of 2024-7075 Aluminium Alloy Sheets Joined by Friction Stir Welding, *Int. J. Mach. Tool. Manuf.*, 2006, **46**, p 588–594
9. J.Q. Su, T.W. Nelson, and C.J. Sterling, Microstructure Evolution During FSW/FSP of High Strength Aluminum Alloys, *Mater. Sci. Eng. A*, 2005, **405**, p 277–286
10. K.V. Jata, K.K. Sankaran, and J.J. Ruschau, Friction-Stir Welding Effects on Microstructure and Fatigue of Aluminum Alloy 7050-T7451, *Metall. Mater. Trans. A*, 2000, **31**, p 2181–2192
11. Y.S. Sato, H. Kokawa, M. Enomoto, and S. Jogan, Microstructural Evolution of 6063 Aluminium During Friction Stir Welding, *Metall. Mater. Trans. A*, 1999, **30**, p 2429–2437
12. N. Kamp, A. Sullivan, and J.D. Robson, Modelling of Friction Stir Welding of 7xxx Aluminium Alloys, *Mater. Sci. Eng. A*, 2007, **466**, p 246–255
13. P. Heurtier, M.J. Jones, C. Desrayaud, J.H. Driver, F. Montheillet, and D. Allehaux, Mechanical and Thermal Modeling of Friction Stir Welding, *J. Mater. Process. Technol.*, 2006, **171**, p 348–357
14. M. Song and R. Kovacevic, Numerical and Experimental Study of the Heat Transfer Process in Friction Stir Welding, *Proc. Inst. Mech. Eng. B: J. Eng. Manuf.*, 2003, **217**, p 73–85
15. *Metals Handbook*, 8th ed., Vol. 8, Metallography, Structures and Phase Diagrams, ASM, Metals Park, OH, 1973, p 124
16. S. Xu and X. Deng, A Study of Texture Patterns in Friction Stir Welds, *Acta Mater.*, 2008, **56**, p 1326–1341
17. F.J. Humphreys and M. Hatherly, *Recrystallization and Related Annealing Phenomena*, 2nd ed., Elsevier, New York, 2005